Journal of Renewable Materials

Tech Science Press

DOI: 10.32604/jrm.2023.021306

ARTICLE

Optimization of Photo-Fenton Catalyst Preparation Based Bamboo Carbon Fiber by Response Surface Methodology

Yizhang Wang[1], Zhaoyang Yu[1], Jinbo Hu[1,2,*], Shanshan Chang[1], Yuan Liu[1], Ting Li[2], Gonggang Liu[1,*] and Xiaodong (Alice) Wang[3]

[1]College of Materials Science and Engineering, Central South University of Forestry and Technology, Changsha, 410004, China

[2]Hunan Taohuajiang Bamboo Science & Technology Co., Ltd., Yiyang, 413400, China

[3]Department of Wood and Forest Sciences, Laval University, Quebec, G1V 0A6, Canada

[*]Corresponding Authors: Jinbo Hu. Email: hjb1999@hotmail.com; Gonggang Liu. Email: liugonggang@csuft.edu.cn

Received: 07 January 2022   Accepted: 01 April 2022

ABSTRACT

In this paper, the residue from bamboo factory has been used to design photo-Fenton catalyst, which has the advantages of low cost and magnetic recycling. The photo-Fenton catalytic performance of the biocarbon-based catalyst was excellent and its optimal preparation process was also explored by response surface methodology. First, bamboo-carbon fiber was selected as the photo-Fenton catalyst carrier. Subsequently, the surface of the carbon fiber was modified, with which dopamine, nano-Fe_3O_4 and nano-TiO_2 were successively loaded by hydrothermal method. After examined single factor tests, four factors including dopamine concentration, ferric chloride mass, P25 titanium dioxide mass and liquid-solid ratio were selected to the characteristic values. The degradation efficiency of photo-Fenton catalyst to methylene blue (MB) solution was treated as the response value. After the analysis of the response surface optimization, it was showed that the significance sequence of the selected 4 factors in terms of the MB degradation efficiency was arranged as following: dopamine concentration > liquid-solid ratio > P25 titanium dioxide quality > ferric chloride quality. The optimal process parameters of fiber-carbon catalyst were affirmed as following: the 1.7 mg/mL concentration of dopamine, the 1.2 g mass of ferric chloride, the 0.2 g mass of P25 titanium dioxide and the liquid-solid ratio of 170 mL/g. The experiment-measured average MB degradation efficiency performed by the optimized catalyst was 99.3%, which was nearly similar to the model-predicted value of 98.9%. It showed that the prediction model and response surface model were accurate and reliable. The results from response surface optimization could provide a good reference to design bamboo-based Fenton-like catalyst with excellent catalytic performance.

KEYWORDS

Photo-fenton catalysis; bamboo fiber; carbon fiber; response surface optimization; methylene blue

1 Introduction

Due to the continuous development of industry dyestuff effluent has grown one of the highly hazardous and difficult-to-treat wastewater in China. Especially organic dyes are characterized by difficult to degrade, toxic and potentially cause cancer, which bring into a huge threat to human health and the living environment [1]. The commonly used treatment methods of dyestuff effluent include physical methods, chemical methods and biological methods, etc. [2]. Advanced oxidation process (AOP) can oxidize large molecules of refractory organics into low-toxic or non-toxic small molecules, which is thought to possess the advantages of high efficient and environmentally friendliness. AOP has widely used to degrade organic dyes in waste water [3]. Photo-Fenton catalytic technology is a kind of AOP by virtue of green light energy, which is generally used in the field of dyestuff effluent treatment. It is as well known that the photo-Fenton catalytic method is a low-cost, no-secondary-pollution and convenient operation [4].

The photo-Fenton system could generate a large number of highly reactive free radicals by the interaction of catalysts, hydrogen peroxide and light, which can decompose the organic dyes in the wastewater into CO_2, H_2O and inorganic substances [5]. Photo-Fenton catalysts has been classified into two categories, namely homogeneous and heterogeneous photo-Fenton catalysts. It has been proved that homogeneous photo-Fenton catalyst has been characterized the strong oxidation ability and high removal rate of refractory substances, however, it is difficult to recycle, separate and operate [6]. The heterogeneous photo-Fenton catalyst has the advantages of high oxidation efficiency, low H_2O_2 consumption, wide effective pH window, easy regeneration and separation, etc. [7–9]. According to the existence form of active ingredients, heterogeneous photo-Fenton catalysts can be divided into unsupported catalysts and supported catalysts [10]. The application of unsupported catalysts has been limited because of the disadvantages of facile agglomeration difficult separation and unrecyclability [11], hence the supported catalysts is popular. The suitable carrier overspreaded with nano-size catalysts could be rendered the photo-Fenton catalyst of degradation efficiency accompanying with the synergistic effects, such as enhancing the light absorption and adsorption enrichment of pollutants.

Nowadays, various catalyst carriers have been used to design high-efficiency photo-Fenton catalyst, especially for carbon materials with excellent light absorption capacity. Graphene oxide coated nano additives of ferric oxide (Fe_3O_4/GO) is employed as the digestion of bisphenol A, that a heterogeneous catalyst for photo-Fenton reaction is prepared by coprecipitation method [12]. Likewise, nano-TiO_2 photocatalyst is fashionably used in photo-Fenton catalysis. Graphene oxide coated ferric oxide and titanium dioxide (Fe_3O_4/GO/TiO_2) is performed to significantly decompose Congo red, which was prepared by hydrothermal method [13]. The multiwalled carbon nanotubes has also been chosen as a photo-Fenton catalyst carrier, which has been designed to attach ferric oxide and TiO_2 as an excellent photo-Fenton catalyst [14,15]. Although graphene, carbon nanotubes and other nanocarriers have been expanded to apply in the catalyst of excellent performance, they have been explored some defects, such as, high prices and difficult recycle. It is not so easy to apply in a large-scale wastewater treatment. In addition, nano-sized catalyst has been detected to potentially have an ecological risk, which would cause secondary pollution to the water body. Hence, biomass-derived carbon as catalyst carrier has been considered a extensive choice due to low cost, renewability, micrometer-scale and good biocompatibility [16–18].

In this study, bamboo-carbon fiber extracted from waste bamboo shavings is investigated as a catalyst carrier. The surface of carbonized-treated fiber is going to modify by polydopamine, which the high-activity functional groups could successively be clad by hydrothermal method, such as nano-Fe_3O_4 and nano-TiO_2. A magnetically recyclable photo-Fenton catalyst could be prepared namely TiO_2/Fe_3O_4/PDA/CF. The preparation process will be emphatically optimized by response surface methodology. The 60-minute degradation efficiency of methylene blue solution (MB) will be taken as the target parameter. The dopamine concentration, the quality of ferric chloride, the quality of P25 nano-TiO_2, and solid-liquid ratio are chosen in the single-factor experiment. Then, the response surface methodology is examined to seek the optimal conditions of catalyst preparation.

2 Materials and Methods

2.1 Chemicals and Materials

Bamboo shavings used in this study was received from Hunan Taohuajiang Bamboo Technology Co., Ltd., China.

NaOH, ascorbic acid, dopamine hydrochloride, Tris-HCl ($NH_2C(CH_2OH)_3{\cdot}HCl$), $FeCl_3{\cdot}6H_2O$, Na_2CO_3, H_2O_2 (30%), methylene blue (MB) and P25 TiO_2 were purchased from Sinopharm Chemical Reagent Co., Ltd. (China) which is used directly.

2.2 Methods

2.2.1 Preparation of Bamboo Fiber

Bamboo shavings were first crushed into 270 μm bamboo powder by a pulverizer. Then 0.5 g of the bamboo powder was placed in a beaker. A 20 mL 6 mol/L NaOH was added to a beaker. Finally, the mixture was put into the hydrothermal reactor for hydrothermal reaction at 160°C for 24 h. It was taken out after cooling, then washed with deionized water until neutral, and then dried for some successive essays.

2.2.2 Preparation of TiO_2/Fe_3O_4/PDA/CF Catalyst

First, the fiber was calcined in an argon atmosphere at 500°C for 2 h to obtain carbon fiber (abbreviated to CF). CFs were immersed into the dopamine hydrochloride solution with Tris-HCl at a pH value of 9 when stirring for 8 h. After that, the deposit of a polydopamine (abbreviated to PDA) layer was anchored on the surface of carbon fibers (abbreviated to PDA/CF). PDA/CF was immersed into $FeCl_3$ solutions in a ultrasound for 30 min, where Na_2CO_3 and ascorbic acid were added. The mixed solution was performed a hydrothermal reaction at 160°C for 24 h (abbreviated to Fe_3O_4/PDA/CF). When Fe_3O_4/PDA/CF was subsequently immersed into NaOH solutions, P25 TiO_2 were added and completed in the hydrothermal reaction at 160°C for 24 h. Finally, the samples were repeatedly washed with deionized water (abbreviated to TiO_2/Fe_3O_4/PDA/CF).

2.2.3 Catalytic Degradation Experiments

0.1 g of the prepared catalyst was added to 200 mL MB solution, that the concentration of MB was 10 mg/L. Then, 0.1 mol/L H_2O_2 solution was added without adjusting the pH value. The beaker holding the mixed solution was lighted by a xenon lamp for 60 min. Here the xenon lamp was simulated the sunlight, which was set to degrade MB. When performed a lighted degradation, the 5 mL solution was taken out by a dropper every 10 min. The 10-minute degraded solution was in sequence centrifuged and gotten the supernatant, which was examined by UV-Vis spectrophotometer. The MB degradation efficiency could be obtained:

$$\text{MB degradation efficiency} = \frac{(C_0 - C_t)}{C_0} \times 100\% \qquad (1)$$

where C_0 and C_t represent the absorbance of MB at initial and desired time intervals. The degradation efficiency of MB in this study was calculated according to formula (1).

2.2.4 Characterization

Morphology of photo-Fenton catalysts were investigated by scanning electron microscope (Nova, Nano SEM230, USA). The photo-Fenton catalysts were examined by XRD analysis, which was the X'Pert X-ray powder diffractometer (D/MAX-2500, Rigaku, Japan) equipped with Cu Kα radiation source. The surface chemical composition and elemental analysis of photo-Fenton catalysts were conducted by X-ray photoelectronic spectroscopy (XPS, Escalab 250 XPS system, Thermo Fisher Scientific UK). The 752N UV-V is spectrophotometer was used to analyze the suspension of treated wastewater sample, which was executed by a detection wavelength at 664 nm corresponding to the maximum absorbance of MB.

3 Results and Discussion

3.1 Characterization of Photo-Fenton Catalysts

In order to further study the microstructure of TiO_2/Fe_3O_4/PDA/CF catalyst, the SEM images of TiO_2/Fe_3O_4/PDA/CF were provided as shown in Figs. 1a–1c. From Figs. 1a, 1b, TiO_2/Fe_3O_4/PDA/CF shows a typical micro-fibrous structure with a diameter of about 2~3 μm. The SEM images of TiO_2/Fe_3O_4/PDA/CF catalyst at a higher magnification large number of nanoparticles and PDA coating are dispersed on the surface of CF as shown in Figs. 1b, 1c. In order to study the chemical composition and nanoparticles distribution, the elemental mapping under the magnifications of Fig. 1c is provided in Figs. 1d–1h. It could be seen that N, Fe, and Ti are homogeneously distributed on the surface of PDA/CF. N element comes from amino groups on modified PDA. Fe and Ti elements come from CF surface loaded nanoparticles. The results show that the nano-Fe_3O_4 and nano-TiO_2 were successfully loaded on the PDA/CF surface.

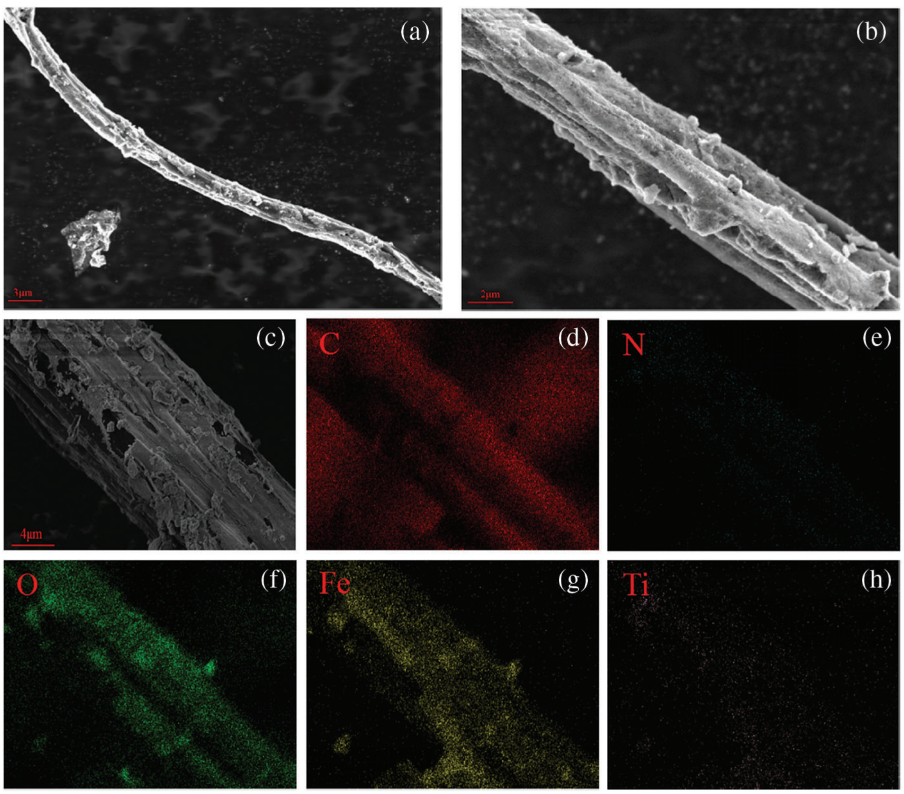

Figure 1: (a, b, c) SEM images of TiO_2/Fe_3O_4/PDA/CF and (d, e, f, g, h) C, N, O, Fe, Ti elemental mapping of TiO_2/Fe_3O_4/PDA/CF

XRD pattern of TiO_2/Fe_3O_4/PDA/CF catalyst is as shown in Fig. 2. Fig. 2 presents to the six typical characteristic peaks 30.2°, 35.5°, 43.2°, 53.5°, 57.1°, and 62.5° which can be assigned to (220), (311), (400), (422), (511) and (440) planes with inverse-spinel structure of Fe_3O_4 (JCPDS no. 19–0629). In addition, Fig. 2 also presents to the three typical characteristic peaks 25.3°, 48.1°, and 62.7° which can be assigned to (101), (200) and (204) planes with anatase of TiO_2 (JCPDS No. 84-1258). It is mainly due to the cladding from nano-Fe_3O_4 and nano-TiO_2 loading. Therefore, XRD results can further prove that the nano-Fe_3O_4 and nano-TiO_2 were successfully loaded on the PDA/CF surface.

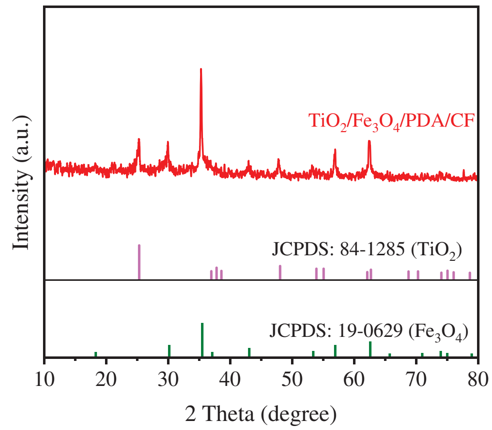

Figure 2: XRD pattern of TiO_2/Fe_3O_4/PDA/CF

The surface chemical compositions of TiO_2/Fe_3O_4/PDA/CF were further investigated by X-ray photoelectron spectroscopy, and the results are shown in Fig. 3. As shown in Fig. 3a, TiO_2/Fe_3O_4/PDA/CF contain O 1s, C 1s, N 1s, Fe 2p, and Ti 2p peaks. It can be seen from the Fig. 3 that the photo-Fenton catalyst contain N, Fe and Ti elements. As shown in Fig. 3b, two typical peaks of Fe 2p states (Fe $2p_{1/2}$ and Fe $2p_{3/2}$) at 723.78 and 710.28 eV were observed for TiO_2/Fe_3O_4/PDA/CF, which is the mixed oxidation state of Fe in Fe_3O_4 [19]. As shown in Fig. 3c, two typical peaks of Ti 2p states (Ti $2p_{1/2}$ and Ti $2p_{3/2}$) at 463.58 and 457.88 eV were observed for TiO_2/Fe_3O_4/PDA/CF, which is the mixed oxidation state of Ti in TiO_2 [20]. The results from XPS spectrum also confirm that the successful PDA modification and nano-Fe_3O_4/TiO_2 loading on the surface of CF.

3.2 Catalytic Performance Analysis

3.2.1 Single-Factor Experiment

The effect of dopamine concentration on the degradation efficiency of MB solution is shown in Fig. 4. The dosage of carbon fiber and ferric chloride are 0.3 and 0.6 g, while the mass of P25 and liquid-solid ratio are 0.05 g and 100. It can be seen from Fig. 4 that the MB degradation efficiency gradually increases when the dopamine concentration changes from 0.5 to 2.5 mg/mL. The maximum value of 97.6% was reached at 2.5 mg/mL, and the degradation efficiency subsequently fluctuated little. This is because the surface of the carbon fiber has fewer functional groups, and the polydopamine modification plays an important role in providing highly active functional groups which allows sufficient loading sites for the loading of inorganic nanoparticles. When the dopamine content is low, the dopamine polymer modified on the surface of the carbon fiber is not dense enough. This will result in insufficient active sites to load subsequent functional nanoparticles. When the dopamine content is further increased, a dense polydopamine coating layer may be formed on the surface of the carbon fiber with saturated active sites. This will allow the subsequent catalyst to have saturated active sites, and the catalytic degradation performance will remain unchanged.

The effect of ferric chloride usage on the degradation efficiency of MB solution is shown in Fig. 5. The dosage of carbon fiber and the dopamine concentration are 0.3 g and 0.5 mg/mL, while the P25 and liquid-to-solid ratio are 0.05 g and 100. It can be seen from Fig. 5 that when ferric chloride usage increases from 0.6 to 1.4 g, the MB degradation efficiency shows a steady upward trend. Then it basically remains unchanged after reaching 1.4 g. The reason is that Fe_3O_4 nanoparticles mainly play the key role of catalytic degradation in the photo-Fenton catalytic system. Ferric chloride is the source of iron for the growth of Fe_3O_4 nanoparticles. When the amount of added ferric chloride is insufficient, a large amount of Fe_3O_4 nanoparticles are difficult to form on the surface of the carbon fiber. This will affect the generation of hydroxyl radicals in catalytic degradation process and lead to the reduction of catalytic activity. When too much ferric chloride is added, the adsorption sites on the surface of the polydopamine modified carbon fiber are close to saturation. This will cause the loading of Fe_3O_4 nanoparticles to remain basically unchanged, making the catalytic degradation performance basically no longer increase.

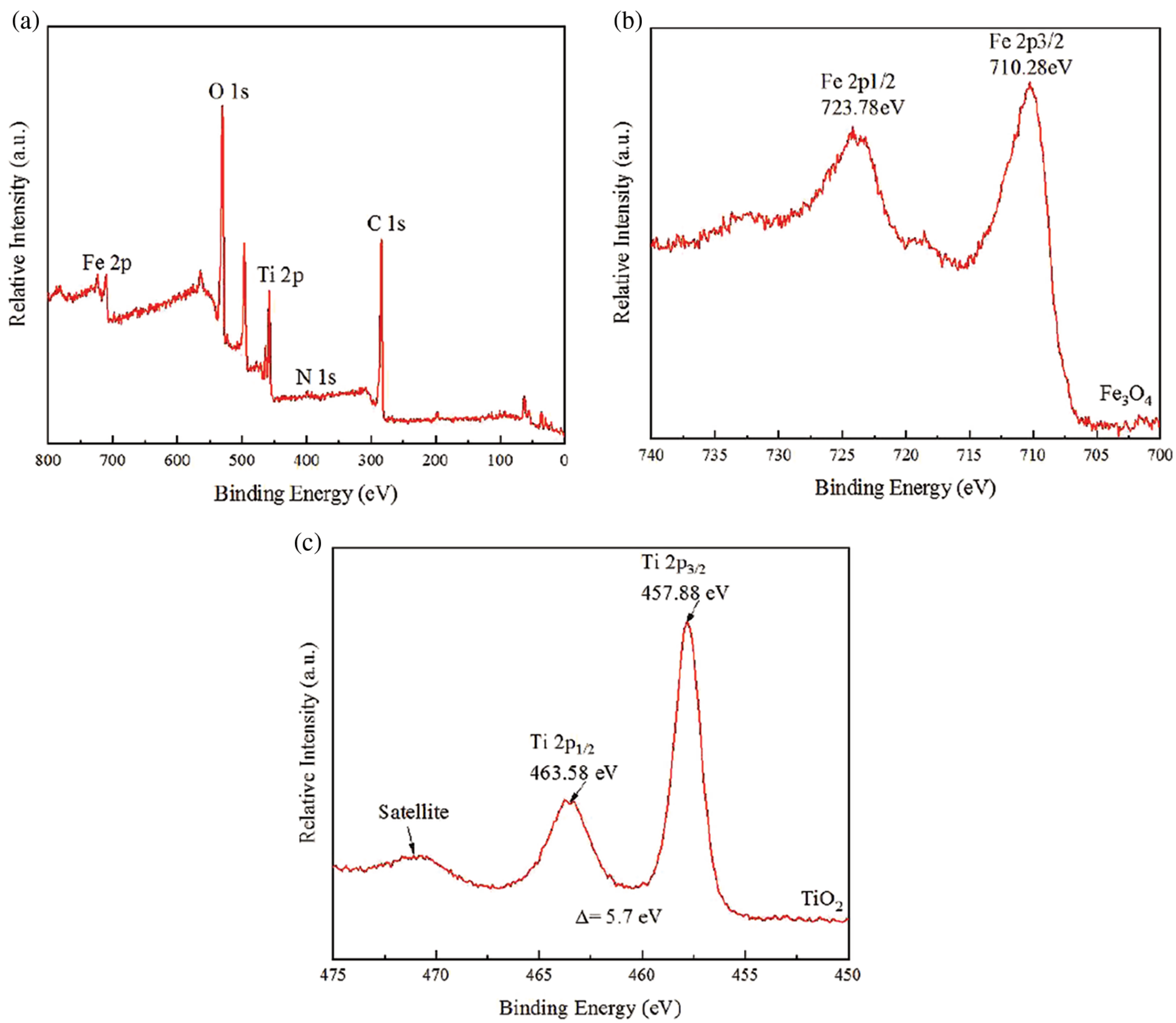

Figure 3: XPS spectra of TiO_2/Fe_3O_4/PDA/CF: (a) the survey scan of TiO_2/Fe_3O_4/PDA/CF, (b) Fe 2p region of TiO_2/Fe_3O_4/PDA/CF, (c) Ti 2p region of TiO_2/Fe_3O_4/PDA/CF

The effect of the mass of P25 on the MB degradation efficiency is shown in Fig. 6. The carbon fiber usage and the dopamine concentration are 0.3 g and 0.5 mg/mL, while the ferric chloride mass and the liquid-to-solid ratio are 0.6 g and 100 mL/g. It can be seen from Fig. 6 that when the mass of P25 increases from 0.05 to 0.25 g, the MB degradation efficiency continues to increase. It reached the maximum value of 99.1% at 0.25 g, and then showed a slow downward trend. The low quality of P25 will affect the amount of formed nano titanium dioxide loaded on the carbon fiber. This will result in low light absorption efficiency in photo-Fenton catalysis. The high quality of P25 results in that part of

P25 cannot be completely dissolved in a strong alkaline solution under high temperature and high pressure, which will be mixed in the prepared catalyst. This will cause the reduction of effective component of TiO_2/Fe_3O_4/PDA/CF which participates in the reaction.

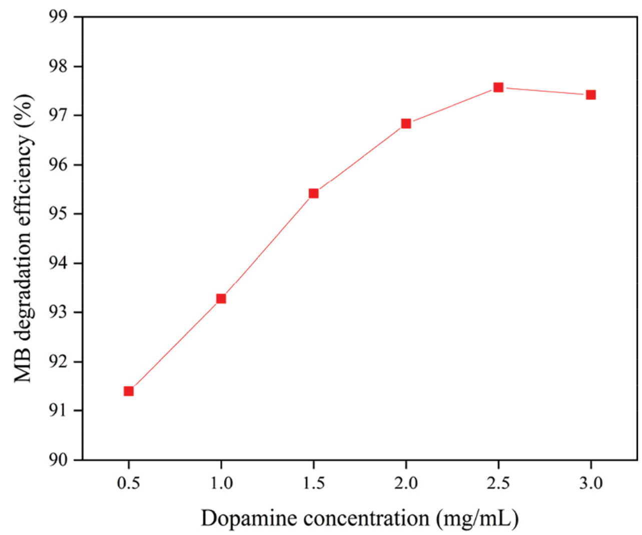

Figure 4: The effect of dopamine concentration on MB degradation efficiency

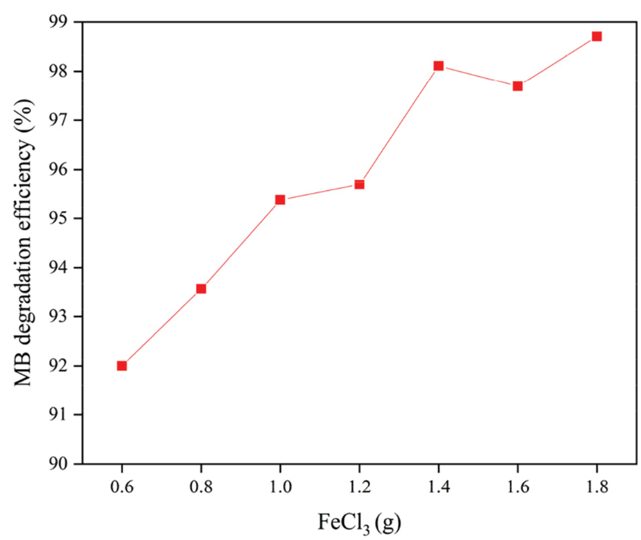

Figure 5: The effect of ferric chloride quality on MB degradation efficiency

The effect of the liquid-solid ration on the MB degradation efficiency is shown in Fig. 7. The carbon fiber usage and the dopamine concentration are 0.3 g and 0.5 mg/mL, while the mass of ferric chloride and P25 are 0.6 g and 0.05 g. It can be seen from Fig. 7 that when the liquid-to-solid ratio increases from 100 to 175 mL/g, the MB degradation efficiency continues to increase. It reached the maximum value of 99.0% at 175 mL/g, and then showed a slow downward trend. Because too little solution will result in too small contact area between liquid phase and solid phase, nanoparticles cannot be completely monodisperse in the solution during the reaction. However, too much solution can lead to the cover of the surface of the photo-Fenton catalyst by residual P25 and ferric chloride, reducing its adsorption performance.

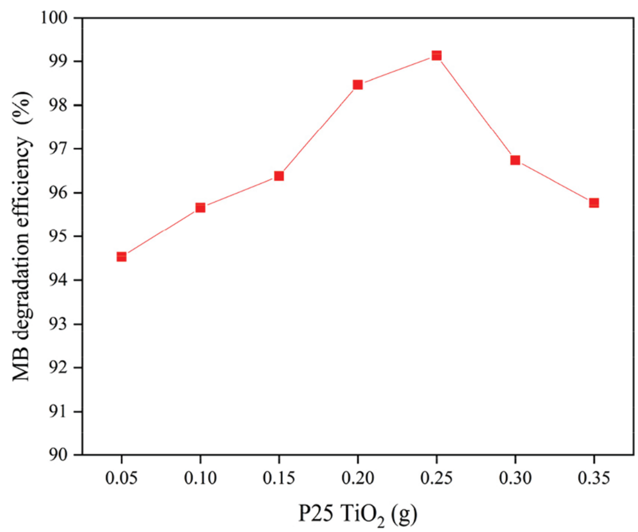

Figure 6: The effect of P25 TiO_2 quality on MB degradation efficiency

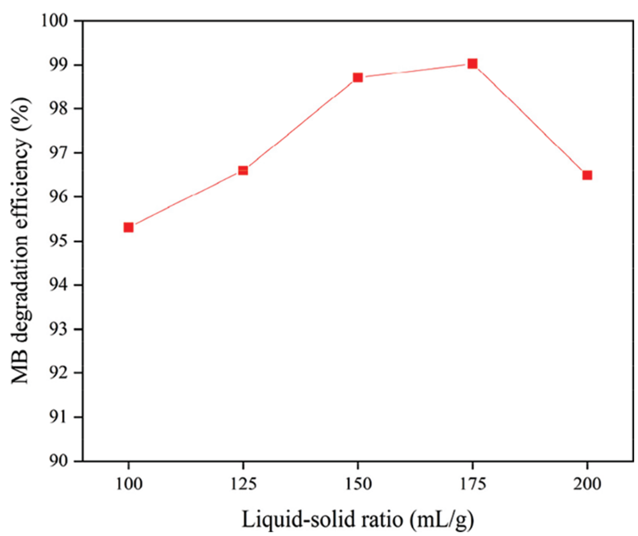

Figure 7: The effect of liquid-solid ratio on MB degradation efficiency

3.2.2 Response Surface Optimization

The optimal conditions obtained in the above single factor experiment did not consider the interaction between the factors. In order to further study the interaction between the factors in the MB degradation efficiency, the response surface analysis method was used to optimize the process conditions. And Box-Behnken experimental design principle was employed in the response surface method. The final MB degradation efficiency after 60 min is selected as the response value, and 4 factors that have an impact on the MB degradation efficiency: dopamine concentration (A), ferric chloride quality (B), P25 quality (C), liquid-solid ratio (D) as the characteristic value, a 4-factor 3-level response surface analysis test was performed, with −1, 0, and 1 respectively representing the level of the variable. The relationship between the 3 level codes of the 4 factors and the test values is presented in Table 1.

Table 1: Factors levels and code of Box-Behnken design

Levels	Dopamine A/(mg/mL)	$FeCl_3$ B/(g)	P25 TiO_2 C/(g)	Liquid-solid ratio D/(mL/g)
−1	0.5	0.6	0.05	100
0	1.5	1.2	0.20	150
1	2.5	1.8	0.35	200

The preparation process of the bamboo fiber-based photo-Fenton catalyst adopts the Box-Behnken experimental design. The final MB degradation efficiency after 60 min is selected as the response value. The response surface experimental results are shown in Table 2.

Table 2: The Box-Behnken design of degradation of MB by photo-Fenton catalyst

No.	Dopamine A/(mg/mL)	$FeCl_3$ B/(g)	P25 TiO_2 C/(g)	Liquid-solid ratio D/(mL/g)	MB degradation efficiency R/(%)
1	0	0	0	0	98.5
2	0	−1	0	−1	93.2
3	0	0	0	0	99.0
4	0	1	1	0	92.7
5	1	0	0	−1	94.3
6	1	0	1	0	94.9
7	1	0	0	1	96.1
8	0	1	0	−1	89.9
9	1	0	−1	0	92.2
10	−1	−1	0	0	90.2
11	−1	0	0	1	94.1
12	1	1	0	0	93.4
13	0	0	1	−1	94.7
14	−1	1	0	0	90.3
15	−1	0	0	−1	91.3
16	0	0	−1	1	94.1
17	−1	0	−1	0	91.0
18	0	−1	1	0	93.2
19	0	0	0	0	97.8
20	−1	0	1	0	90.2
21	1	−1	0	0	92.3
22	0	0	0	0	98.1
23	0	0	0	0	99.0

(Continued)

Table 2 (continued)

No.	Dopamine A/(mg/mL)	$FeCl_3$ B/(g)	P25 TiO_2 C/(g)	Liquid-solid ratio D/(mL/g)	MB degradation efficiency R/(%)
24	0	1	0	1	95.3
25	0	−1	0	1	92.9
26	0	0	1	1	96.4
27	0	−1	−1	0	91.3
28	0	1	−1	0	90.5
29	0	0	−1	−1	92.5

Use Design-Expert 10.0.3 software to analyze the experimental data and get the quadratic polynomial regression equation:

MB degradation efficiency (R) = 98.452 + 1.33917A − 0.08B + 0.868333C + 1.07917D + 0.25

25AB + 0.8775AC − 0.2675AD + 0.08BC + 1.4175BD + 0.0425CD − 3.23767A2 − 3.86642B2 − 2.81142C2 − 1.41267D2.

As presented in Table 3, analysis of variance (ANOVA) was used to test the importance level of this model. The F value can be used to test the significance of the impact of each variable on the response value. The larger the F value, the higher the significance of the corresponding variable. When the model's significance test probability is $P < 0.05$, the model is considered to be statistically significant. It can be seen from Table 3 that the order of the influence of process conditions on MB degradation efficiency is: A > D > C > B, that is, dopamine concentration > liquid-solid ratio > P25 quality > ferric chloride quality. The coefficient of determination R^2 of the model is 0.9777, indicating that the model is highly significant. $R^2adj = 0.9554$, which can explain 95.5% of the experimental response value variation. R^2 is close to the predicted correlation coefficient Pred R^2, indicating that the experimental model fits well with the real data and has practical guiding significance. Therefore, the response surface optimization model can be used to design and optimize experimental conditions.

Table 3: ANOVA data for the model of degradation of MB by photo-Fenton catalyst

Source	Sum of squares	Freedom degree	Variance	F-value	P-value	Significance
Model	215.06	14	15.36	43.81	<0.0001	**
A	21.52	1	21.52	61.38	<0.0001	**
B	0.077	1	0.077	0.22	0.6470	
C	9.05	1	9.05	25.81	0.0002	**
D	13.98	1	13.98	39.86	<0.0001	**
AB	0.26	1	0.26	0.73	0.4081	
AC	3.08	1	3.08	8.78	0.0103	*
AD	0.29	1	0.29	0.82	0.3815	
BC	0.026	1	0.026	0.073	0.7909	
BD	8.04	1	8.04	22.92	0.0003	**
CD	7.225E − 003	1	7.225E − 003	0.021	0.8879	
A^2	67.99	1	67.99	193.92	<0.0001	**
B^2	96.97	1	96.97	276.55	<0.0001	**

(Continued)

Table 3 (continued)

Source	Sum of squares	Freedom degree	Variance	*F*-value	*P*-value	Significance
C^2	51.27	1	51.27	146.22	<0.0001	**
D^2	12.94	1	12.94	36.92	<0.0001	**
Residual	4.91	14	0.35			
Lack of fit	3.71	10	0.37	1.24	0.4521	
Pure error	1.20	4	0.30			
Total	219.97	28				

Note: $R^2 = 0.9777$, $R_2adj = 0.9554$, Pred $R^2 = 0.8943$.

It can be seen from Fig. 8 that the influence trend of the interaction between dopamine concentration and ferric chloride quality on the MB degradation efficiency presents a parabolic surface distribution. The MB degradation efficiency first increased and then decreased with the increase of dopamine concentration and ferric chloride quality. Dopamine concentration causes greater fluctuations in the curved surface that first increases and then decreases, indicating that it has a more significant impact on the MB degradation efficiency. Because the surface of carbon fiber is inert and has fewer active functional groups, while dopamine contains more active functional groups including amino and phenolic hydroxyl [21]. The surface modification and adhesion of dopamine can form a polydopamine coating on the surface of carbon fibers and provide highly active functional groups, which can provide adsorption sites for the loading of more inorganic nanoparticles [22,23]. On the other hand, carbon fibers with a polydopamine coating layer can promote the dispersion and anchoring of inorganic nanoparticles. This can also avoid agglomeration between particles and meet the requirements of high dispersion and low agglomeration of catalyst nanoparticles [24,25]. Dopamine modifies the surface of carbon fibers to form a polydopamine coating, which can prevent the agglomeration of Fe_3O_4 nanoparticles [26,27]. The Fe_3O_4 nanoparticles can be uniformly loaded on the surface of the carbon fiber, and the degradation ability of the catalyst can be improved. Hence, under moderate conditions which dopamine concentration and ferric chloride mass are 1.5–2.0 mg/mL and 1.0–1.3 g, the MB degradation efficiency can be significantly increased.

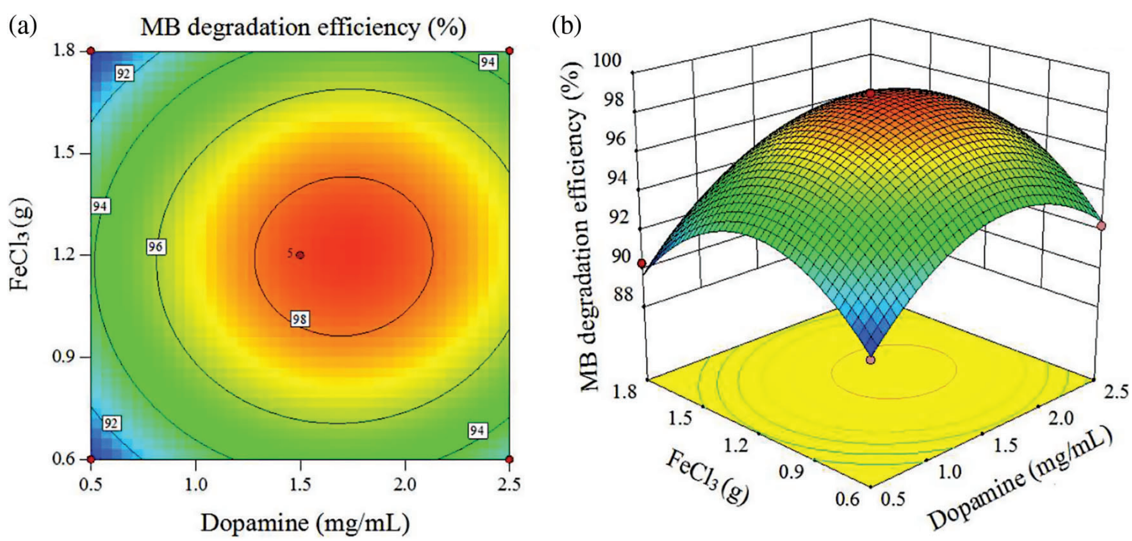

Figure 8: Interaction between dopamine concentration and $FeCl_3$ quality (a) Plane contour map and (b) Stereo response surface map

Fig. 9 shows the three-dimensional curved surfaces and contours of the influences of two factors on the MB degradation efficiency. It can be seen from Fig. 9 that the two-factor interactive surface has a large longitudinal span and the contour line is obviously elliptical. It shows that the interaction of the two factors has a significant impact on the MB degradation efficiency. TiO_2 nanoparticles loading on the surface of carbon fibers could be formed via the dissociation and reorganization of the crystal structure of P25 in a concentrated alkaline solution [28]. And the modification of carbon fiber by polydopamine can increase the loading content of formed TiO_2 nanoparticles on the surface of carbon fiber. On the other hand, the polydopamine coating of carbon fiber can also prevent agglomeration between TiO_2 nanoparticles. Hence, the modification of dopamine plays a key role in the uniform and firm loading of nanoparticles on the surface of carbon fibers. Therefore, the influence of dopamine plays a major role, and the fluctuation range caused by it will be slightly larger. The results of MB degradation efficiency showed a first increase and then a decrease with the increase of dopamine concentration and P25 titanium dioxide mass. Therefore, under moderate conditions which dopamine concentration and P25 mass are 1.5–2.0 mg/mL and 0.17–0.29 g, the MB degradation efficiency can be significantly increased.

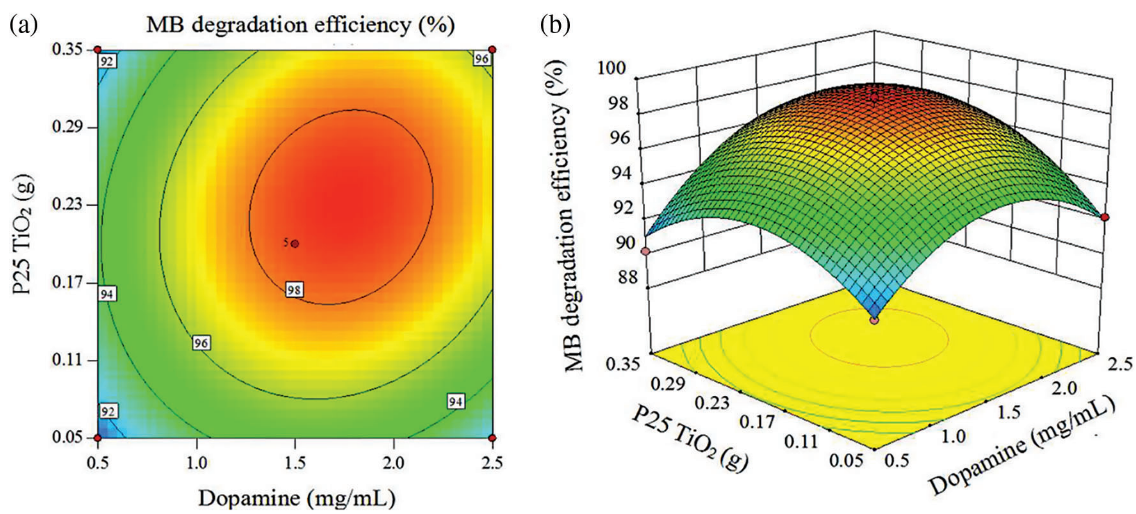

Figure 9: Interaction between dopamine concentration and P25 TiO_2 quality (a) Plane contour map and (b) Stereo response surface map

It can be seen from Fig. 10 that the MB degradation efficiency first increased and then decreased with the increase of dopamine concentration and liquid-solid ratio. Dopamine concentration has a greater change in MB degradation efficiency, indicating that dopamine concentration has a more significant impact on MB degradation efficiency. Both Fe_3O_4 and TiO_2 nanoparticles are prepared by in situ loading on carbon fiber by hydrothermal method. Liquid-solid ratio refers to the ratio of the added solution to the mass of carbon fiber, and has nothing to do with the liquid concentration. Therefore, dopamine is an important factor for the uniform and abundant loading of Fe_3O_4 and TiO_2 nanoparticles on the surface of carbon fibers, leading to greater fluctuations caused by dopamine.

It can be seen from Fig. 11 that when the mass of ferric chloride is less than 1.2 g, the MB degradation efficiency is positively correlated with it. When the mass of ferric chloride is greater than 1.2 g, the correlation will change. When the mass of ferric chloride is around 1.2 g, this is the critical optimum process parameter of MB degradation efficiency. In the same way, the critical optimum parameter of MB degradation efficiency changing with the quality of P25 TiO_2 is about 0.23 g. This may be because the $FeCl_3$ solution realizes the in-situ loading of Fe_3O_4 nanoparticles on the surface of the carbon fiber by the hydrothermal reaction and the contained Fe^{2+} oxidizes to Fe^{3+} at a faster rate. However, Fe^{3+} continues to react with H_2O_2 and $\cdot HO_2$ to form Fe^{2+}, so it is a continuous cycle of Fe^{3+}/Fe^{2+} and H_2O_2. This shows that nano-Fe_3O_4 is extremely important. The reaction process is as follows [29,30]: $Fe^{2+} + H_2O_2 \rightarrow Fe^{3+} + (OH)^- + \cdot OH$, $H_2O_2 + Fe^{3+} \rightarrow Fe^{2+} + \cdot HO_2 + H^+$, $Fe^{2+} + \cdot OH \rightarrow Fe^{3+} + (OH)^-$, $Fe^{3+} + \cdot HO_2 \rightarrow Fe^{2+} + O_2 + 2H^+$. In the photo-Fenton catalytic system, nano-TiO_2 can absorb ultraviolet rays and accelerate the reaction rate [31,32]. Nano TiO_2 could produce electron-hole pairs after absorbing ultraviolet rays. These electron-hole pairs migrate to the surface of nano-TiO_2 and react with organic matter on the surface of nano-TiO_2 to produce hydroxyl radicals [33]. These hydroxyl radicals from nano-TiO_2 and the hydroxyl radicals generated by the nano-Fe_3O_4 catalysis together play a catalytic degradation effect, so the reaction efficiency is accelerated. Both have a significant impact on the MB degradation efficiency, so there is little difference in the fluctuation range caused.

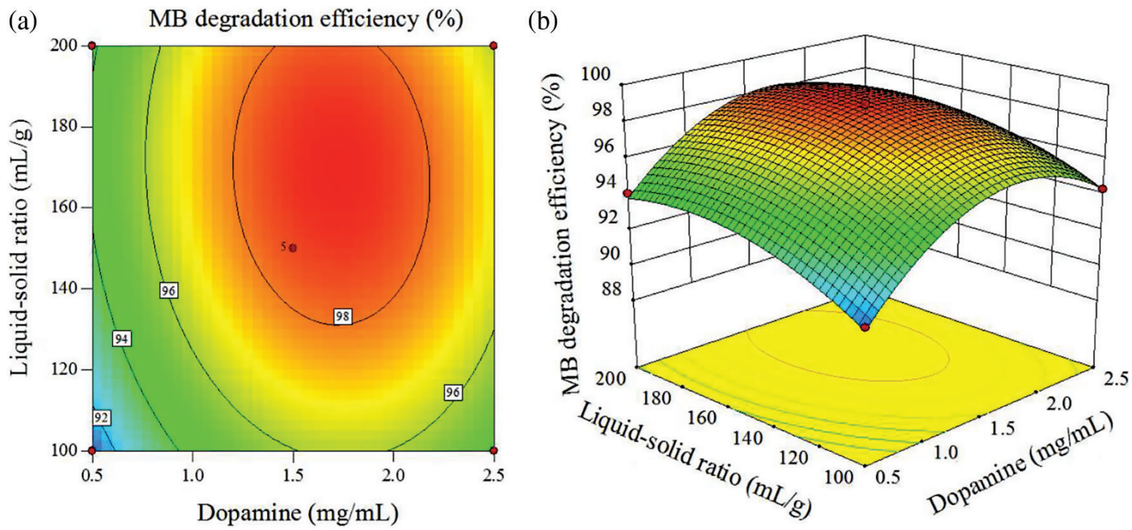

Figure 10: Interaction between dopamine concentration and liquid-solid ratio (a) Plane contour map and (b) Stereo response surface map

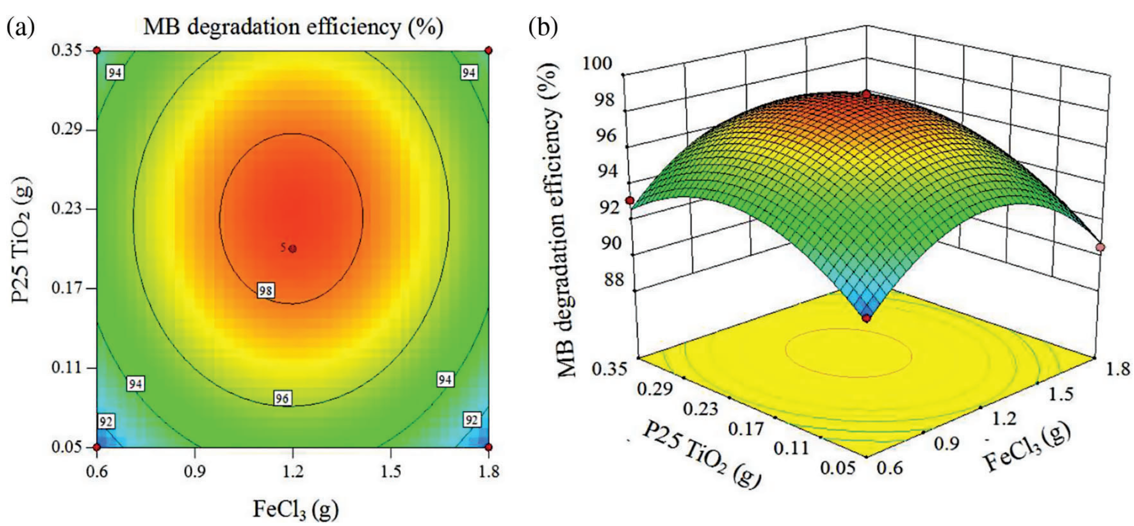

Figure 11: Interaction between quality of ferric chloride and the quality of P25 titanium dioxide (a) Plane contour map and (b) Stereo response surface map

As shown in Figs. 12a and 12b, the ferric chloride quality and the liquid-solid ratio are 0.9–1.5 g and 140–200 mL/g. This is the maximum distribution area of the curved surface, which is beneficial to promote the increasing degradation efficiency of MB. As shown in Figs. 12c and 12d, MB degradation efficiency first increases and then decreases with the increase of P25 mass and liquid-to-solid ratio. Take the moderate level combination: the quality of P25 is 0.23 g and the liquid-solid ratio is around 160 mL/g, which can significantly increase the MB degradation efficiency. This is because when the liquid-solid ratio and the mass of $FeCl_3$ and P25 increased, the MB degradation efficiency showed a trend of first increasing and then decreasing. This increases the internal diffusion resistance [34,35], resulting in that $FeCl_3$ and P25 are not completely monodispersed in the solution after ultrasound. When the solvent is too much, the content of other impurities will increase with the increasing [36,37]. This will affect the loading of Fe_3O_4 and TiO_2 nanoparticles. However, Fe_3O_4 and TiO_2 nanoparticles play the main role in photo-Fenton catalysis, which causes the fluctuations caused by $FeCl_3$ and P25 TiO_2 to be greater than those caused by the liquid-solid ratio.

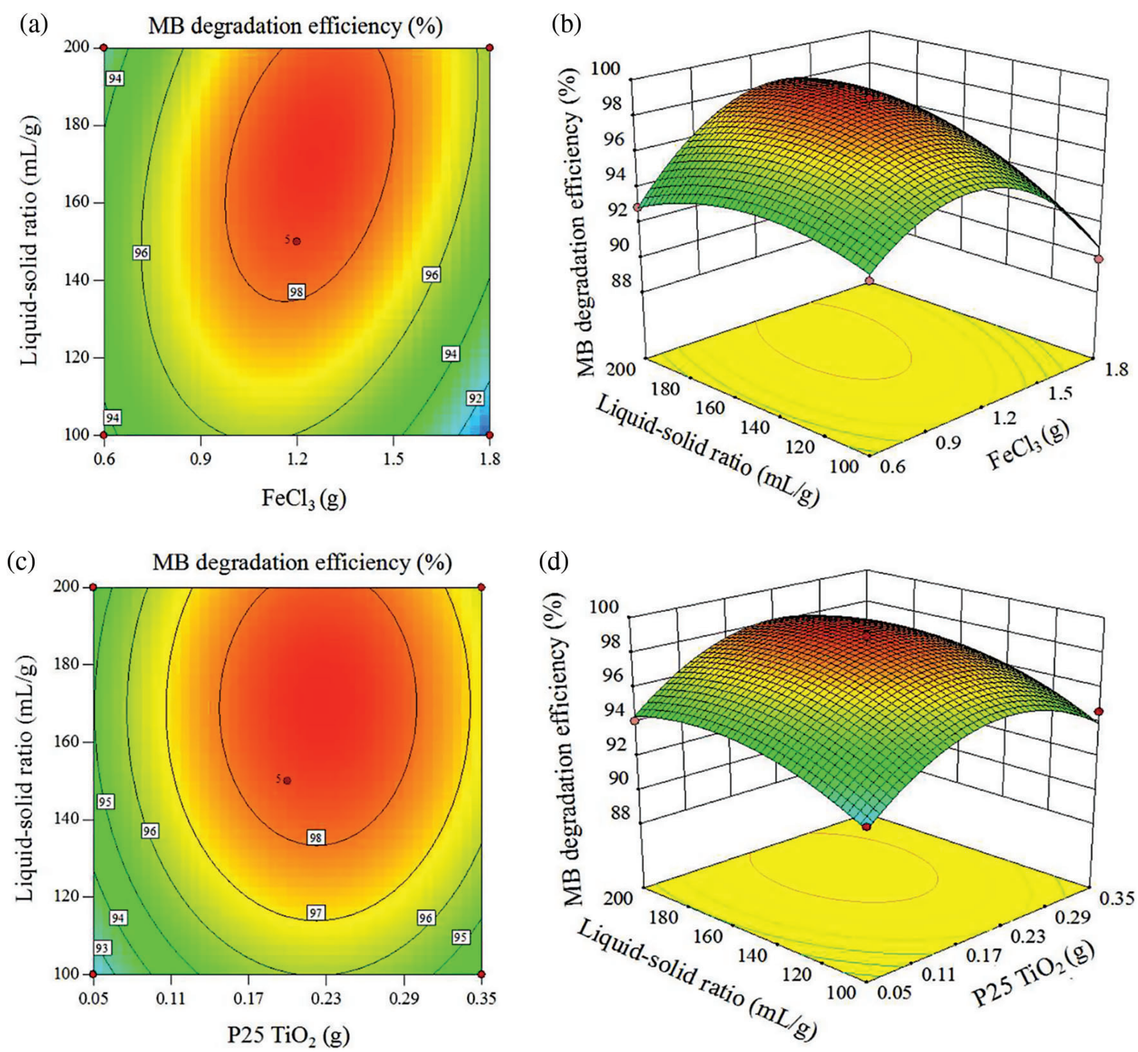

Figure 12: Interaction between ferric chloride quality, P25 titanium dioxide quality and liquid-solid ratio (a, c) Plane contour map and (b, d) Stereo response surface map

In order to synergistically consider the influence of the interaction between various factors on the MB degradation efficiency, the global optimal solution was further determined. According to the results of the Design-Expert 10.0.3 software, the maximum MB degradation efficiency is selected as the optimization goal. The optimal processes under the combined influence of multiple factors such as dopamine concentration, ferric chloride quality, P25 quality and liquid-solid ratio are as follows: dopamine concentration 1.720 mg/mL, ferric chloride quality 1.243 g, P25 quality 0.229 g, liquid-solid ratio 170.055 mL/g. Under these conditions, the MB degradation efficiency predicted by the model is 98.9%.

In order to verify the reliability of the model and the feasibility in practice, actual experiment was carried out. According to the results of the software prediction, three parallel tests were performed on the conditions of dopamine concentration 1.7 mg/mL, ferric chloride mass 1.2 g, P25 titanium dioxide mass 0.2 g, and liquid-solid ratio 170 mL/g. The experimental result shows that the average MB degradation efficiency is 99.3%, which is close to the model prediction result. This result shows that the response surface model analysis and optimization method of photo-Fenton catalyst based on bamboo carbon fiber are effective and feasible, and the model can better reflect the relationship between MB degradation efficiency and various selected factors.

3.2.3 Photo-Fenton Catalytic Mechanism of Catalysts

The MB degradation efficiency curves under different systems are presented in Fig. 13. It can be seen from Fig. 13 that under the condition of only Xenon lamp irradiation and only H_2O_2, the MB degradation efficiency are only 14.3% and 2.80% after 1 h. This result indicates that MB degrades slowly under Xenon lamp irradiation, and the degradation efficiency of MB is low in the absence of light. When photo-Fenton catalyst was added with only Xenon lamp irradiation or only H_2O_2, the degradation efficiency of MB reached 32.1% and 30.6%, respectively. The results showed that the degradation efficiency of MB was improved to a certain extent. When TiO_2/Fe_3O_4/PDA/CF catalyst was used as a photo-Fenton catalyst in presence of light and H_2O_2, the degradation efficiency of MB was significantly increased and it reaches 98.2% after 1 h reaction. The results indicate TiO_2/Fe_3O_4/PDA/CF catalyst has a higher photo-Fenton catalytic activity for degradation of MB than single Fenton and photocatalytic reaction. In order to study the effect of adsorption performance on the enhanced photo-Fenton catalytic activity of TiO_2/Fe_3O_4/PDA/CF catalyst, its adsorption performance without light and H_2O_2 is displayed. The results show that the removal rate of MB reached 12.2% after 1 h. It is proved that good adsorption ability in favor of increasing photo-Fenton catalytic activity of TiO_2/Fe_3O_4/PDA/CF catalyst. On the other hand, the photo-Fenton catalytic activity of TiO_2/Fe_3O_4/CF catalyst without PDA modification was studied. This proves the positive role of PDA. The results show that the degradation efficiency of MB reached 64.2% after 1 h. It is proved that the TiO_2/Fe_3O_4/CF catalyst without PDA modification has a decent photo-Fenton catalytic activity, but it is far behind TiO_2/Fe_3O_4/PDA/CF catalyst. This experiment further confirms that PDA modification to CF can enhance its photo-Fenton catalytic activity which is mainly due to realize the uniform and firm loading of nanoparticles on the surface of CF. Besides, the photo-Fenton catalytic activity of Fe_3O_4/PDA/CF catalyst without loading of nano-TiO_2 was studied. The results show that the degradation efficiency of MB reached 87.6% after 1 h. It is proved that the Fe_3O_4/PDA/CF catalyst without loading of nano-TiO_2 also has a decent photo-Fenton catalytic activity, but it lags behind TiO_2/Fe_3O_4/PDA/CF catalyst. The result further confirms that loading of nano-TiO_2 can enhance the photo-Fenton catalytic activity of TiO_2/Fe_3O_4/PDA/CF catalyst which is mainly due to realizing light absorption enhancement by loading nano-TiO_2 on the surface of CF.

The effects of different capturing agents on the degradation efficiency of TiO_2/Fe_3O_4/PDA/CF catalyst were also discussed. The results are presented in Fig. 14. TEA, BQ and MeOH are added in the photo-Fenton reaction system as hole trapping agent, superoxide radical trapping agent and hydroxyl radical trapping agent, respectively. From Fig. 14, when no trapping agents were added, the degradation efficiency of MB reached 98.2% after 1 h. And TEA has a promoting effect on degradation efficiency of MB. The degradation efficiency of MB reached 94.6% after 40 min. After 40 min, the degradation efficiency of MB changed little and remained stable. BQ almost had no obvious effect on degradation efficiency of MB. The MB degradation efficiency reached 95.3% after 1 h. It indicates hole trapping is beneficial to the enhancement of degradation efficiency of MB while superoxide radical has no obvious effect on photo-Fenton catalytic degradation reaction. But a severe inhibitory effect could be observed when adding MeOH. The degradation efficiency of MB only reached 74.8% after 1 h. The result proves that hydroxyl radicals play a crucial role in the photo-Fenton catalytic degradation reaction.

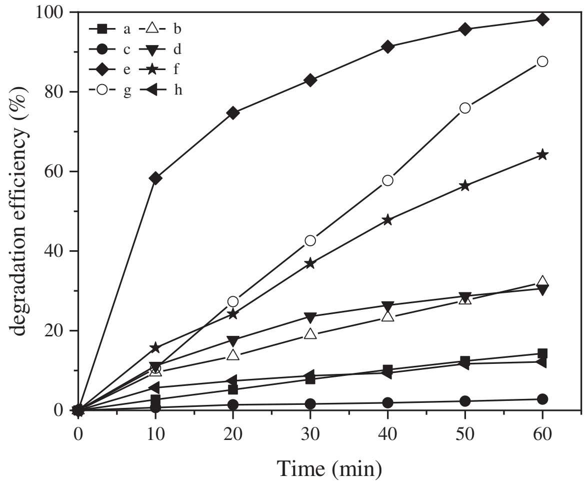

Figure 13: MB degradation efficiency curves in different reaction systems: (a, c) only light or H_2O_2 without catalyst, (b, d) TiO_2/Fe_3O_4/PDA/CF catalyst with only light or H_2O_2 (e) TiO_2/Fe_3O_4/PDA/CF catalyst with light and H_2O_2, (f) TiO_2/Fe_3O_4/CF catalyst with light and H_2O_2, (g) Fe_3O_4/PDA/CF catalyst with light and H_2O_2, (h) only TiO_2/Fe_3O_4/PDA/CF catalyst

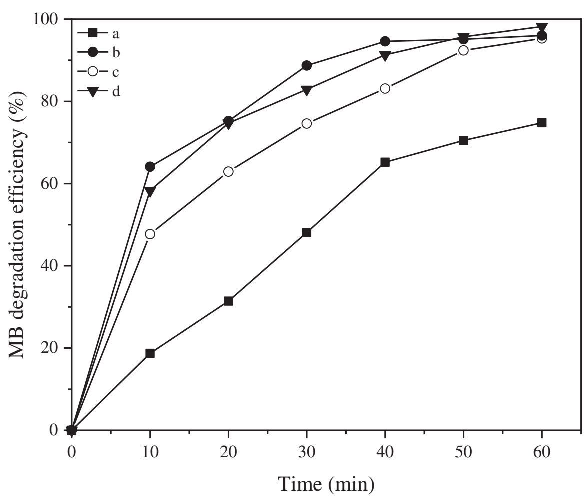

Figure 14: The effect of different trapping agents on degradation efficiency of TiO_2/Fe_3O_4/PDA/CF catalyst: (a) MeOH, (b) TEA, (c) BQ, (d) without any trapping agents

4 Conclusions

In this study, the residue from bamboo factory has been used to design photo-Fenton catalyst, which has the advantages of low cost and magnetic recycling. The bamboo-carbon fiber extracted from waste bamboo shavings is investigated as a catalyst carrier. The surface of carbonized-treated fiber is going to modify by polydopamine, which the high-activity functional groups could successively be clad by hydrothermal method, such as nano-Fe_3O_4 and nano-TiO_2. A magnetically recyclable photo-Fenton catalyst could be prepared namely TiO_2/Fe_3O_4/PDA/CF. After the analysis of the response surface optimization, it was showed that the significance sequence of the selected 4 factors in terms of the MB degradation efficiency was arranged as following: dopamine concentration > liquid-solid ratio > P25 titanium dioxide quality > ferric chloride quality. The optimal process parameters of fiber-carbon catalyst were affirmed as following: the 1.7 mg/mL concentration of dopamin, the 1.2 g mass of ferric chloride, the 0.2 g mass of P25 titanium dioxide and the liquid-solid ratio of 170 mL/g. The experiment-measured average MB degradation efficiency performed by the optimized catalyst was 99.3%, which was nearly similar to the model-predicted value of 98.9%. This result proves that the prediction model and response surface model were accurate and reliable. It not only provided low-cost, high-efficiency and large-scale applied photo-Fenton catalyst in water treatment, but also realized high-value and green utilization of bamboo waste.

Authors' Contributions: Yizhang Wang: Experiment and Writing-Original Draft. Jinbo Hu and Shanshan Chang: Supervision, Writing-Reviewing and Editing. Gonggang Liu and Xiaodong (Alice) Wang: Data Curation. Zhaoyang Yu and Ting Li: Resources. Yuan Liu: Investigation.

Acknowledgement: Dr. Jinbo HU would like to thank Prof. Xiangzhi SONG in Faculty of Chemistry and Chemical Engineering, Central South University.

Funding Statement: The study received the funding from Hunan Provincial Key Research and Development Program (2020WK2018), Hunan Provincial Forestry Technological Innovation Funds (XLK202107-3), Scientific Research Project of Hunan Education Department (19A505, 21B0242), National Natural Science Foundation of China (No. 21908251), Hunan Provincial Natural Science Foundation of China (No. 2020JJ2058).

Conflicts of Interest: The authors declare that they have no conflicts of interest to report regarding the present study

References

1. Donkadokula, N. Y., Kola, A. K., Naz, I., Saroj, D. (2020). A review on advanced physico-chemical and biological textile dye wastewater treatment techniques. *Reviews in Environmental Science and Bio/Technology, 19(3),* 543–560. DOI 10.1007/s11157-020-09543-z.
2. Ahmed, S., Rasul, M. G., Martens, W. N., Brown, R., Hashib, M. A. (2011). Advances in heterogeneous photocatalytic degradation of phenols and dyes in wastewater: A review. *Water Air Soil Pollution, 215(1–4),* 3–29. DOI 10.1007/s11270-010-0456-3.
3. Ma, D. S., Yi, H., Lai, C., Liu, X. G., Huo, X. Q. et al. (2021). Critical review of advanced oxidation processes in organic wastewater treatment. *Chemosphere, 275,* 130104. DOI 10.1016/j.chemosphere.2021.130104.
4. Kumar Shivappa Masalvad, S., Kumar Sakare, P. (2020). Application of photo-Fenton process for treatment of textile Congo-red dye solution. *Materials Today: Proceedings, 46,* 5291–5297. DOI 10.1016/j.matpr.2020.08.650.
5. Kiziltas, H., Tekin, T., Tekin, D. (2020). Preparation and characterization of recyclable Fe_3O_4@SiO_2@TiO_2 composite photocatalyst, and investigation of the photocatalytic activity. *Chemical Engineering Communications, 208(7),* 1–13. DOI 10.1080/00986445.2020.1743694.
6. Herney-Ramirez, J., Vicente, M. A., Madeira, L. M. (2010). Heterogeneous photo-Fenton oxidation with pillared clay-based catalysts for wastewater treatment: A review. *Applied Catalysis B Environmental, 98(1–2),* 10–26. DOI 10.1016/j.apcatb.2010.05.004.

7. Miralles-Cuevas, S., Oller, I., Pérez, J. A. S., Malato, S. (2014). Removal of pharmaceuticals from MWTP effluent by nanofiltration and solar photo-Fenton using two different iron complexes at neutral pH. *Water Research, 64,* 23–31. DOI 10.1016/j.watres.2014.06.032.
8. Giannakis, S. (2017). Analogies and differences among bacterial and viral disinfection by the photo-Fenton process at neutral pH: A mini review. *Environmental Science and Pollution Research, 25(28),* 27676–27692. DOI 10.1007/s11356-017-0926-x.
9. Fayazi, M. (2021). Preparation and characterization of carbon nanotubes/pyrite nanocomposite for degradation of methylene blue by a heterogeneous Fenton reaction. *Journal of the Taiwan Institute of Chemical Engineers, 120,* 229–235. DOI 10.1016/j.jtice.2021.03.033.
10. Kakavandi, B., Babaei, A. A. (2016). Heterogeneous Fenton-like oxidation of petrochemical wastewater using a magnetically separable catalyst (MNPs@c): Process optimization, reaction kinetics and degradation mechanisms. *RSC Advances, 6(88),* 84999–85011. DOI 10.1039/C6RA17624K.
11. Kocijan, M., Ćurković, L., Ljubas, D., Mužina, K., Bačić, I. et al. (2021). Graphene-based TiO_2 nanocomposite for photocatalytic degradation of dyes in aqueous solution under solar-like radiation. *Applied Sciences, 9(11),* 3966. DOI 10.3390/app11093966.
12. Hua, Z. L., Ma, W. Q., Bai, X., Feng, R. R., Yu, L. et al. (2014). Heterogeneous Fenton degradation of bisphenol A catalyzed by efficient adsorptive Fe_3O_4/GO nanocomposites. *Environmental Science and Pollution Research, 21(12),* 7737–7745. DOI 10.1007/s11356-014-2728-8.
13. Zhang, L., Cai, Y., Huang, C. M., Chen, K. Z., Xiao, K. J. et al. (2018). Degradation of Congo Red by a new photo-Fenton catalyst of Fe_3O_4@GO@TiO_2. *Environmental Science & Technology, 41(6),* 57–62. DOI 10.19672/j.cnki.1003-6504.2018.06.010.
14. Shi, T., Peng, J., Chen, J. Q., Sun, C., He, H. (2017). Heterogeneous photo-Fenton degradation of norfloxacin with Fe_3O_4-multiwalled carbon nanotubes in aqueous solution. *Catalysis Letters, 147(6),* 1598–1607. DOI 10.1007/s10562-017-2026-4.
15. Zhang, K., Meng, Z. D., OH, W. (2010). Degradation of Rhodamine B by Fe-carbon nanotubes/TiO_2 composites under UV light in aerated solution. *Chinese Journal of Catalysis, 31(7),* 751–758. DOI 10.1016/S1872-2067(09)60084-X.
16. Hu, M., Wang, C., Lu, C., Anuar, N. I. S., Yousfani, S. H. S. et al. (2020). Investigation on the classified extraction of the bamboo fiber and its properties. *Journal of Natural Fibers, 17(12),* 1798–1808. DOI 10.1080/15440478.2019.1599311.
17. Yang, Q. X., Yu, L. J., Dong, Y. B., Fu, Y. Q., Zhu, Y. F. (2020). Preparation and microwave absorption properties of magnetic functional porous biomass carbon composites. *Carbon, 158,* 931. DOI 10.1016/j.carbon.2019.10.094.
18. Bai, S. Z., Wang, T. T., Tian, Z. S., Cao, K. S., Li, J. T. (2020). Facile preparation of porous biomass charcoal from peanut shell as adsorbent. *Scientific Reports, 10(1),* 15845. DOI 10.1038/s41598-020-72721-0.
19. Stefan, M., Leostean, C., Pana, O., Toloman, D., Popa, A. et al. (2016). Magnetic recoverable Fe_3O_4-TiO_2: Eu composite nanoparticles with enhanced photocatalytic activity. *Applied Surface Science, 390,* 248–259. DOI 10.1016/j.apsusc.2016.08.084.
20. Leostean, C., Pana, O., Stefan, M., Popa, A., Toloman, D. et al. (2018). New properties of Fe_3O_4@SnO_2 core shell nanoparticles following interface charge/spin transfer. *Applied Surface Science, 427,* 192–201. DOI 10.1016/j.apsusc.2017.07.267.
21. Jang, J., Song, S. H., Kim, H., Moon, J., Ahn, H. et al. (2021). Janus graphene oxide sheets with Fe_3O_4 nanoparticles and polydopamine as anodes for lithium-ion batteries. *ACS Applied Materials & Interfaces, 13(12),* 14786–14795. DOI 10.1021/acsami.1c02892.
22. Zhou, L., Xu, K. Z., Zhu, H., Liu, C. H., Duan, J. Y. et al. (2020). Magnetic microsphere with hierarchical LDH/polydopamine shell encapsulated Fe_3O_4 core for carrying Ag nanocatalyst. *Colloids and Surfaces A: Physicochemical and Engineering Aspects, 601,* 125022. DOI 10.1016/j.colsurfa.2020.125022.
23. Zeng, Y. B., Zhou, Y., Kong, L., Zhou, T. S., Shi, G. Y. (2013). A novel composite of SiO_2-coated graphene oxide and molecularly imprinted polymers for electrochemical sensing dopamine. *Biosensors and Bioelectronics, 45,* 25–33. DOI 10.1016/j.bios.2013.01.036.

24. Zhai, X. R., Cheng, S. Y., Wang, H., Zhang, C., Li, Y. et al. (2021). Fast preparation of Fe_3O_4@polydopamine/Au for highly efficient degradation of tetracycline. *Chemosphere, 285,* 131523. DOI 10.1016/j.chemosphere.2021.131523.

25. Mohanta, D., Ahmaruzzaman, M. (2021). Facile fabrication of novel Fe_3O_4-SnO_2-gC_3N_4 ternary nanocomposites and their photocatalytic properties towards the degradation of carbofuran. *Chemosphere, 285,* 131395. DOI 10.1016/j.chemosphere.2021.131395.

26. Abbasi-Asl, H., Sabzehmeidani, M. M., Ghaedi, M. (2021). Efficient degradation of metronidazole antibiotic by TiO_2/Ag_3PO_4/g-C_3N_4 ternary composite photocatalyst in a continuous flow-loop photoreactor. *Journal of Environmental Chemical Engineering, 9(5),* 105963. DOI 10.1016/j.jece.2021.105963.

27. Wang, W., Zhou, S. X., Li, R., Peng, Y. J., Sun, C. et al. (2021). Preparation of magnetic powdered carbon/nano-Fe_3O_4 composite for efficient adsorption and degradation of trichloropropyl phosphate from water. *Journal of Hazardous Materials, 416,* 125765. DOI 10.1016/j.jhazmat.2021.125765.

28. Xu, D., Ma, H. L. (2021). Degradation of rhodamine B in water by ultrasound-assisted TiO_2 photocatalysis. *Journal of Cleaner Production, 313,* 127758. DOI 10.1016/j.jclepro.2021.127758.

29. Fuku, K., Kanai, H., Todoroki, M., Mishima, N., Akagi, T. et al. (2021). Heterogeneous fenton degradation of organic pollutants in water enhanced by combining iron-type layered double hydroxide and sulfate. *Chemistry-an Asian Journal, 16(14),* 1887–1892. DOI 10.1002/asia.202100375.

30. Boutemedjet, A., Djerad, S., Tifouti, L., Bachari, K. (2021). Effect of Fe^0 content on the effectiveness of Fe^0/Fe_3O_4 catalyst in fenton process. *Journal of Water Process Engineering, 41,* 102079. DOI 10.1016/j.jwpe.2021.102079.

31. Hu, F. G., Sun, S. P., Xu, H. L., Li, M. L., Hao, X. F. et al. (2021). Investigation on g-C_3N_4/rGO/TiO_2 nanocomposite with enhanced photocatalytic degradation performance. *Journal of Physics and Chemistry of Solids, 156,* 110181. DOI 10.1016/j.jpcs.2021.110181.

32. Zhou, X., Zhou, M., Ye, S. J., Xu, Y. B., Zhou, S. Q. et al. (2021). Antibacterial activity and mechanism of the graphene oxide (rGO)-modified TiO_2 catalyst against enterobacter hormaechei. *International Biodeterioration & Biodegradation, 162,* 105260. DOI 10.1016/j.ibiod.2021.105260.

33. Ma, B. R., Xin, S. S., Ma, X. M., Zhang, C. L., Gao, M. C. (2021). Preparation of ternary reduced graphene oxide/ BiOBr/TiO_2 nanotube arrays for photoelectrocatalytic degradation of p-chloronitrobenzene under visible light irradiation-sciencedirect. *Applied Surface Science, 551,* 149480. DOI 10.1016/j.apsusc.2021.149480.

34. Henych, J., Štastný, M., Němeková, Z., Mazanec, K., Tolasz, J. et al. (2021). Bifunctional TiO_2/CeO_2 reactive adsorbent/photocatalyst for degradation of bis-p-nitrophenyl phosphate and CWAs. *Chemical Engineering Journal, 414(3),* 128822. DOI 10.1016/j.cej.2021.128822.

35. Alsaffar, M. A., Rashid, S. A., Ayodele, B. V., Hamidon, M. N., Yasin, F. M. et al. (2020). Response surface optimization of multilayer graphene growth on alumina-supported bimetallic cobalt–nickel substrate. *Arabian Journal for Science and Engineering, 45,* 7455–7465. DOI 10.1007/s13369-020-04586-4.

36. Jitjamnong, J., Thunyaratchatanon, C., Luengnaruemitchai, A., Kongrit, N., Kasetsomboon, N. (2020). Response surface optimization of biodiesel synthesis over a novel biochar-based heterogeneous catalyst from cultivated (*Musa sapientum*) banana peels. *Biomass Conversion and Biorefinery, 11(6),* 1–17. DOI 10.1007/s13399-020-00655-8.

37. Wang, C., Shen, Z. P., Cui, X., Jiang, Y. H., Jiang, X. L. (2020). Response surface optimization of enzyme-assisted extraction of R-phycoerythrin from dry *Pyropia yezoensis*. *Journal of Applied Phycology, 32,* 1429–1440. DOI 10.1007/s10811-019-01963-x.